Brownian particles in transient polymer networks

Joris Sprakel,* Jasper van der Gucht, and Martien A. Cohen Stuart
Laboratory of Physical Chemistry and Colloid Science, Wageningen University, Dreijenplein 6, 6703 HB Wageningen, The Netherlands

Nicolaas A. M. Besseling
Section NanoStructured Materials, Department of Chemical Engineering, Delft University of Technology, Julianalaan 136, 2628 BL Delft, The Netherlands

(Received 28 November 2007; published 3 June 2008)

We discuss the thermal motion of colloidal particles in transient polymer networks. For particles that are physically bound to the surrounding chains, light-scattering experiments reveal that the submillisecond dynamics changes from diffusive to Rouse-like upon crossing the network formation threshold. Particles that are not bound do not show such a transition. At longer time scales the mean-square displacement (MSD) exhibits a caging plateau and, ultimately, a slow diffusive motion. The slow diffusion at longer time scales can be related to the macroscopic viscosity of the polymer solutions. Expressions that relate the caging plateau to the macroscopic network elasticity are found to fail for the cases presented here. The typical Rouse scaling of the MSD with the square root of time, as found in experiments at short time scales, is explained by developing a bead-spring model of a large colloidal particle connected to several polymer chains. The resulting analytical expressions for the MSD of the colloidal particle are shown to be consistent with experimental findings.

DOI: 10.1103/PhysRevE.77.061502 PACS number(s): 05.40.Jc, 82.70.Dd, 83.80.−k

I. INTRODUCTION

Microrheology is a growing field of science, founded on the pioneering work of researchers such as Weitz and Mason [1,2] and MacKintosh and Schmidt [3,4]. In microrheology, the thermal motion of probe particles is interpreted in terms of the mechanical properties of the medium in which they are suspended. The motion of the particles can be quantified with a variety of techniques, such as diffusing wave spectroscopy [5], dynamic light scattering [6], and various microscopy-based techniques [7], often in combination with tools such as optical tweezers [8]. Besides the study of synthetic model systems, such as polymer solutions [9], associative polymer networks [10], and living polymer systems [6], the field has found a connection with biology in the numerous publications on biological materials such as actin networks [11], microtubule solutions [12], and membranes [13].

In order to relate measurements of particle dynamics to the macroscopic viscoelastic moduli, Mason and Weitz assumed that the Stokes drag for viscous fluids can be extended to describe the viscoelastic drag at all frequencies [1]. The generalized Stokes-Einstein relation that they proposed assumes furthermore that the medium is homogeneous around the particle and that it can be considered as a viscoelastic continuum. This seems justified if the particle radius R is much larger than the bulk correlation length ξ of the medium. Nevertheless, significant differences between bulk rheology and microrheology have been observed even for $R > \xi$ [6,10]. It has been argued that such discrepancies could be related to depletion layers around the particles [14–16]. The occurrence of depletion should be very sensitive to specific interactions between the particles and the medium. In this paper we analyze in detail how such interactions affect the dynamics of colloidal particles embedded in transient polymer networks, in particular at short times.

Since Einstein's famous paper on Brownian motion [17], it is known that the mean-square displacement $\langle \Delta r^2 \rangle$ of colloidal particles in purely viscous fluids increases linearly with time, the diffusion coefficient being the proportionality constant. The motion of colloids in viscoelastic media, however, is more complex. Most types of motion show scaling behavior:

$$\langle \Delta r^2 \rangle \propto t^{\alpha}. \tag{1}$$

For diffusion, $\alpha = 1$. All dynamics for which the exponent α is smaller than unity, are denoted subdiffusive. According to the generalized Stokes-Einstein relation used in microrheology, such subdiffusive behavior can be related to the viscoelastic response of the medium at the corresponding frequencies [1]. For example, for particles in elastic media with $G^*(\omega) = G_0$, caging is observed ($\alpha = 0$); i.e., the particles are restricted to displacements for which the elastic deformation energy of the surrounding matrix is smaller than the thermal energy $k_B T$, leading to a plateau in the mean-square displacement [18]. Another example of subdiffusive behavior was observed for particles in solutions of F-actin, where $\alpha = 0.75$ is found at short times. This can be related to the $G^*(\omega) \propto \omega^{3/4}$ behavior predicted for semiflexible polymers at high frequencies [11]. For beads covalently bound to microtubules, α was found to depend on the flexibility of the chains; "relaxed" chains yield $\alpha = 0.8$, whereas prestretched, hence more rigid, microtubules gave significantly lower values of α [12]. Finally, subdiffusive behavior may also be caused by local structural inhomogeneities in the medium, unrelated to the bulk rheology. For example, particles in F-actin networks were seen to "hop" between distinct pores in the network, giving $0 < \alpha < 1$, depending on the ratio R/ξ [19].

*Also at Dutch Polymer Institute (DPI), P.O. Box 902, 5600 AX Eindhoven, The Netherlands. Joris.Sprakel@wur.nl

Recently, we have reported evidence of a Rouse-like motion ($\alpha=\frac{1}{2}$) of colloidal particles that are physically bound to flexible polymer networks [20]. In this paper we present a detailed analysis of this type of submillisecond dynamics of colloidal particles in transient polymer networks. The experimental results are rationalized by constructing an analytical model for the motion of a large colloidal particle connected to a surrounding polymer network. We also discuss the motion of the probe particles at intermediate (milliseconds) and longer (seconds) time scales, and compare these to predictions based on the bulk rheological behavior of the solutions.

II. EXPERIMENT

A. Materials

Hydroxy-terminated polyethylene oxide (PEO), with a nominal M_W of 35 kg/mol and $M_W/M_N=1.2$, was used as purchased from Fluka. Part of it was converted into a telechelic associative polymer by attaching hexadecyl ($C_{16}H_{33}$) groups at the chain ends, as follows. The PEO was reacted in toluene with hexadecyl isocyanate (Sigma) in the presence of dibutyl tindilaurate [DBTDL] (Sigma), at 60 °C for 12 h. After three cycles of dissolution in toluene and precipitation in heptane, the polymer was further purified by dissolution in ethyl acetate, filtration over 0.2-μm syringe filters, evaporation of the solvent, and drying. Critical chromatography indicated that approximately 85% of all chain ends have been modified with a hexadecyl tail; i.e., on average, 1.7 hydrophobic groups are attached per chain.

Silica particles (Monospher M100, Merck) with a hydrodynamic radius of 70 nm are used either without further treatment (denoted plain silica particles) and after a preadsorption step with a high-molecular-weight PEO (referred to as PEO-covered silica in the remainder of this paper). This treatment involved diluting the silica particles to a 1 wt % dispersion, adding 10 mg/l of polyethylene oxide (Polymer Source), with a molecular weight of 1000 kg/mol, and stirring for 72 h. Highly monodisperse, charge-stabilized core-shell latex particles ($R_h=110$ nm), polymerized from styrene and some acidic acrylate monomers, where kindly supplied by Akzo Nobel Coatings Research (Sassenheim, the Netherlands). The silica particles (plain and PEO covered) are used at a volume fraction of 10^{-4} and the latex particles at a volume fraction of 10^{-5}, such that particle-particle interactions are negligible and multiple scattering is avoided.

The dynamic light-scattering experiments are carried out on three different setups: (a) a homebuilt setup equipped with a diode-pumped solid-state (DPSS) laser ($\lambda=532$ nm), a photomultiplier tube (PMT) detector, and hardware correlator, with a fixed detection angle of 90°; (b) an ALV5000, equipped with an argon laser ($\lambda=514.5$ nm), ALV/SO-SIPD fiber detector mounted on a goniometer and a hardware correlator; and (c) a Malvern Nano-S, with a He-Ne laser ($\lambda=632.8$ nm), an avalanche photodetector at a detection angle of 173°. In all experiments the temperature was controlled at 20 °C.

Rheological measurements are conducted on a Paar Physica MCR301 rheometer. The viscosity measurements are carried out in a couette (concentric cylinder) geometry at shear rates well within the Newtonian regime of the corresponding system. The viscoelastic properties of the networks are characterized in oscillatory experiments in a cone-plate setup with a cone diameter of 75 mm. In these experiments the frequency of deformation is varied at a fixed strain of 10%, which was checked to be in the linear regime. For both geometries the temperature was kept at 20 °C with integrated peltier elements.

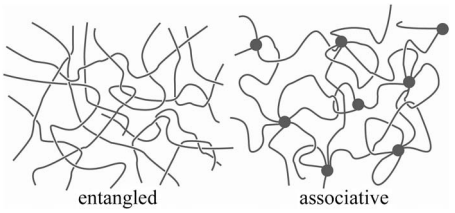

FIG. 1. Schematic representation of the two types of networks that are discussed in this paper. On the left a solution of flexible polymers above the overlap concentration, in which the junction points are formed by entanglements. On the right a micellar, associative network of telechelic polymers. In these associative networks the junction points are formed by flowerlike micelles, that are interconnected by polymer bridges [20].

B. Classification of systems

We study the motion of colloidal particles in two classes of transient polymer networks; see Fig. 1. The first are entangled systems of flexible homopolymers. We use aqueous solutions of polyethylene oxide (PEO). The second class of networks are associative networks formed from the $C_{16}H_{33}$-modified telechelic associative polymers described above. These types of polymers are known to form transient networks, in which the nodes are flowerlike micelles, interconnected by polymer bridges [21].

In this study we distinguish two types of particle-matrix interactions, as illustrated in Fig. 2. (i) *Sticking particles*: when the polymer chains in the network can adsorb onto the particle surface. In this study we use plain silica particles; it is well-known that PEO strongly adsorbs onto silica surfaces [22]. (ii) *Nonsticking particles*: when the polymer chains in the network cannot adsorb onto the particle surface. For the

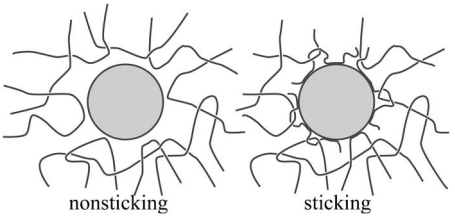

FIG. 2. Schematic illustration of the two types of particle-network interactions. On the left the "nonstick" situation, in which no chains of the matrix adsorb onto the particle. This situation also applies when adsorbed chains are not entangled or associated with the matrix. On the right "sticking" between particle and matrix as a result of adsorption of polymer chains onto the particle surface. These adsorbed chains are connected to the transient network, either through entanglements or through associative interactions [20].

entangled polymer networks these are the latex particles, and in the associative networks these are the PEO-covered silica particles; in this case, the high-molecular-weight PEO layer adsorbed onto the particles ensures that the chains in the network cannot adsorb [23]. The high-molecular-weight polymers that are adsorbed onto these particles can, however, participate in entanglements, which will also become important in the associative networks at higher concentrations.

C. Dynamic light scattering

The mean-square displacement (MSD) $\langle \Delta r^2 \rangle$ of monodisperse spherical particles can be measured directly with dynamic light scattering (DLS) [24]. The intensity correlation function $g^{(2)}(t)$ evaluates fluctuations in the intensity I of light scattered by the particles:

$$g^{(2)}(t) = \frac{\langle I(\tau) I(\tau + t) \rangle}{\langle I(\tau) \rangle^2}. \tag{2}$$

From $g^{(2)}(t)$ one obtains the normalized field autocorrelation function $g^{(1)}(t)$:

$$g^{(2)}(t) = 1 + A[g^{(1)}(t)]^2, \tag{3}$$

where $0 < A \leq 1$ is an instrumental constant. Assuming Gaussian statistics, $g^{(1)}(t)$ gives direct access to the MSD of the particles using

$$\langle \Delta r^2(t) \rangle = \frac{-6}{q^2} \ln[g^{(1)}(t)], \tag{4}$$

where $q = 4\pi n_m \sin(\theta/2)/\lambda$ is the length of the scattering vector, with θ the angle of detection measured with respect to the incident beam, n_m the refractive index of the medium, and λ the wavelength of the light in vacuum. Use of Eq. (4) is justified when the scattering of the polymer matrix is negligible with respect to that of the particles and when particle-particle interactions can be ignored. The particle concentrations in our experiments are chosen such that both requirements are obeyed.

In Fig. 3 we have plotted the MSD, at several fixed times, versus the measurement angle in the light-scattering setup, expressed as the scattering vector q. We see that the MSD [Eq. (4)] is almost constant over the investigated q range, which indicates that non-Gaussian contributions to the particle displacement are small. The small deviations from the dotted horizontal lines, as seen in Fig. 3, must be attributed to minor errors in the alignment of the optical train in the light-scattering setup. These errors however do not influence the results shown below, as these are obtained at fixed scattering angles.

In the setups used here, the shortest available correlation time is 200 ns. Our data, which was recorded during 2 h or more per sample, starts at 10 μs and ends at 100 s, hence well within the borders of the accessible range of correlation times. The accuracy of the normalized correlation function $g^{(2)}(t) - 1/A$ can be estimated using an approximation given by Berne and Pecora [25]. For a measurement of 2 h, which is the minimum here, the standard deviation in the correlation function is approximately $(1 \times 10^{-5})\%$ for $\tau = 10$ μs and 0.1% for $\tau = 100$ s. Hence, the data presented here are accurate over the entire time range investigated. Note that this DLS technique offers a significantly higher short-time resolution than video-based particle-tracking methods [26].

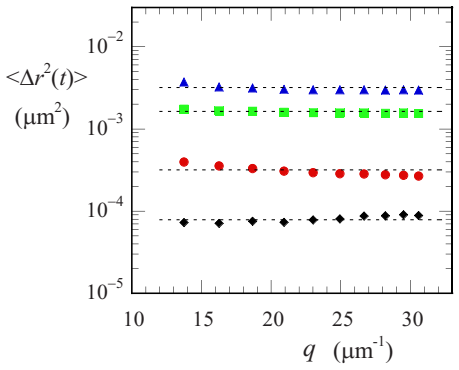

FIG. 3. (Color online) Angular dependence of the MSD of plain silica particles ($R_h = 70$ nm) in a 80-g/l aqueous solution of PEO ($M_W = 35$ kg/mol) at a given correlation time t. The angle of detection was varied between 50° and 140° on light-scattering setup No. 2 and is expressed here as the scattering vector q. Shown are $t = 10^{-2}$ ms (♦), $t = 10^{-1}$ ms (●), $t = 1$ ms (■), and $t = 2$ ms (▲).

III. RESULTS AND DISCUSSION

A. Linear rheology of polymer solutions

For both polymer classes we have measured the low shear viscosity η as a function of polymer concentration in the absence of particles. The results are shown in Fig. 4. At low polymer concentrations the viscosity increases very weakly with polymer concentration. At a certain concentration, the increase in viscosity becomes much stronger. We will loosely denote this concentration as the network formation threshold (where the network can be formed by micellar junction points in the case of the telechelic polymers or by entanglements in the case of unmodified PEO). For the unmodified PEO, this occurs at approximately 25 g/l, and the crossover from the dilute to the entangled regime is rather gradual. For the associative polymers this occurs at a significantly lower

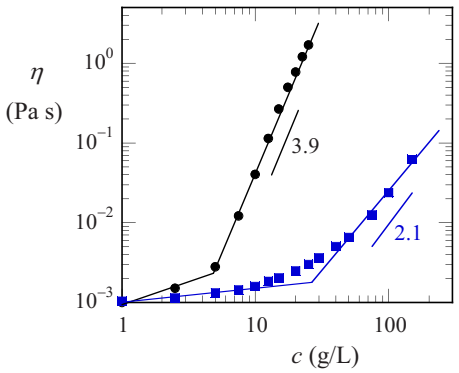

FIG. 4. (Color online) Low shear viscosities of aqueous solutions of PEO [$M_W = 35$ kg/mol (■)] and aqueous solutions of hexadecyl ($C_{16}H_{33}$)-modified PEO of the same molecular weight (●). Drawn lines are power-law fits to the experimental data.

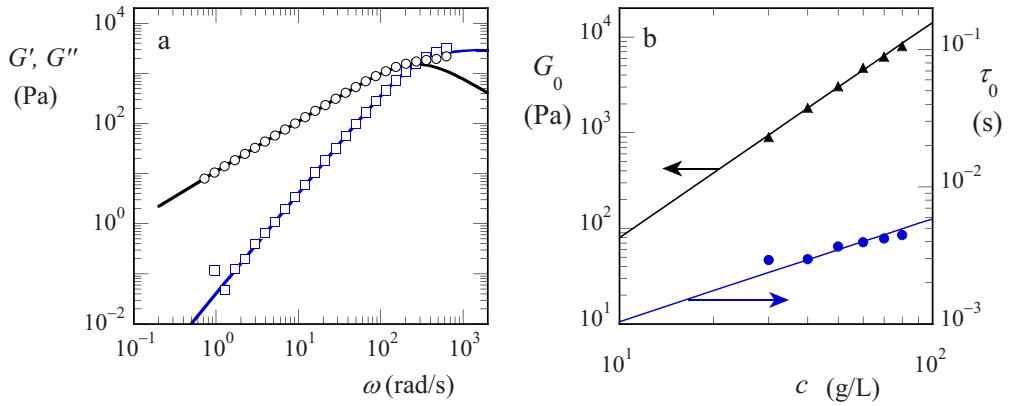

FIG. 5. (Color online) (a) Frequency dependence of storage [G' (□)] and loss [G'' (◯)] moduli of a 50-g/l aqueous solution of associative polymers. Drawn lines are fits to the Maxwell model [Eqs. (5) and (6)]. (b) Plateau modulus [G_0 (▲)] and relaxation time [τ_0 (●)] versus associative polymer concentration. Drawn lines are power-law fits to the data, with $G_0 \propto c^{2.3}$ and $\tau_0 \propto c^{0.75}$.

concentration of 5 g/l and the transition is much sharper. Figure 4 also shows that the viscosity increase beyond this network threshold is stronger for the associative networks ($\eta \propto c^{3.9}$) than for the entangled systems ($\eta \propto c^{2.1}$). This is due to the difference in network structure and strength of the junction points.

In rheological oscillation measurements the viscoelastic properties of a system can be determined. In these measurements, the storage (G') and loss (G'') moduli are determined as a function of the angular deformation frequency ω. For the associative system, a typical result is show in Fig. 5(a). The simplest description of a viscoelastic fluid is the spring-dashpot model, or so-called Maxwell model, which is governed by a single relaxation time τ_0 [27]. The Maxwell model leads to the following expressions for the storage modulus,

$$G' = \frac{G_0 \tau_0^2 \omega^2}{1 + \omega^2 \tau_0^2}, \tag{5}$$

and loss modulus,

$$G'' = \frac{G_0 \tau_0 \omega}{1 + \omega^2 \tau_0^2}, \tag{6}$$

where G_0 is the plateau modulus. The mechanical response of the associative networks is described well by the Maxwell model, as seen from the fit to Eqs. (5) and (6) in Fig. 5(a). The Maxwell behavior of associative polymer systems has been established extensively in the literature [28].

The values of G_0 and τ_0, obtained in this manner for the associative polymer system, are plotted in Fig. 5(b) as a function of polymer concentration. In classical transient network theories, such as the generalized Green-Tobolsky theory of Tanaka and Edwards [29], the plateau modulus is linearly proportional to the number of elastically active chains. When the fraction of all chains that are elastically active is constant, we would also expect a linear relation between plateau modulus and concentration. We observe a much stronger increase in G_0 with concentration, however: $G_0 \propto c^{2.3}$. Annable *et al.* [28] gave an explanation in terms of structural changes of the network; i.e., not only does the total number of chains in the system increase with concentration, but also the fraction of those chains that are mechanically active.

B. Motion of particles in polymer solutions

The primary result of the light-scattering experiments are the intensity correlation functions [Eq. (2)]. In Fig. 6 we show a set of such correlation functions for plain silica particles in associative networks. For particles in pure water, we see a monoexponential decay, which is indicative of purely diffusive motion of monodisperse particles. With increasing polymer concentration the main relaxation time shifts to higher values, as a result of the increasing viscosity of the medium (as shown in Fig. 4). At higher polymer concentrations the correlation functions start to deviate from a simple monoexponential decay. This complex behavior will become more apparent when the results are converted into the MSD $\langle \Delta r^2(t) \rangle$, using Eq. (4).

In Fig. 7 some typical results are shown. For particles in pure water, here shown for both plain silica particles [Fig. 7(a)] and for PEO-covered silica particles [Fig. 7(b)], the

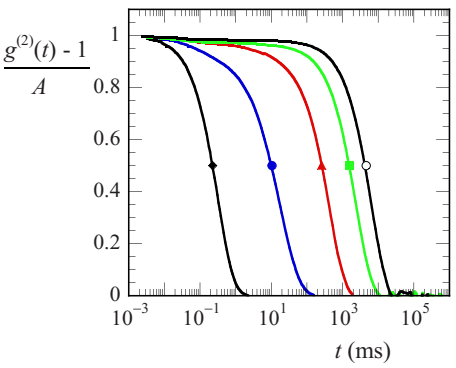

FIG. 6. (Color online) Normalized intensity correlation functions, as obtained with DLS, of plain silica particles (R_h=70 nm) in aqueous solutions of associative polymers as a function of polymer concentration: 0 g/l (♦), 9.6 g/l (●), 30.1 g/l (▲), 49.5 g/l (■), and 77.1 g/l (◯). Each curve consists of approximately 250 data points [20].

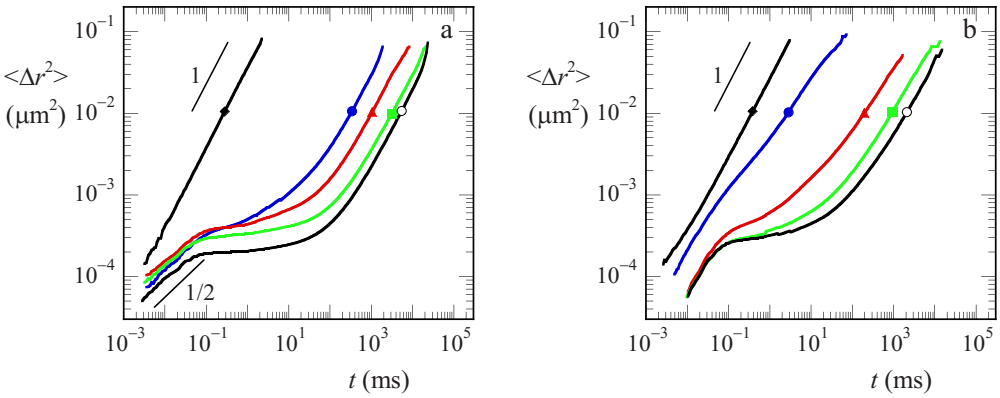

FIG. 7. (Color online) MSD of colloids in associative networks, as measured with DLS [Eq. (4)]. (a) Sticking conditions: plain silica particles (R_h=70 nm) in associative polymer solutions of 0 (♦), 20.0 g/l (●), 30.1 g/l (▲), 49.9 g/l (■), and 60.2 g/l (◯). (b) Nonstick conditions: silica particles pretreated with a high-molecular-weight PEO in associative polymer solutions of 0 (♦), 10.0 g/l (●), 19.9 g/l (▲), 30.1 g/l (■), and 40.0 g/l (◯).

monoexponential decay in the correlation curves corresponds to a linear relation between the MSD and time. This is the sign of pure diffusion, where the exponent α in Eq. (1) is 1. The proportionality constant in this relation is $6D$, where D is the diffusion coefficient [17].

When the pure water that surrounds the particles is replaced by a polymer network, the behavior becomes more complex. For nonsticking particles in a polymer solution that has formed a transient network, as shown in Fig. 7(b), we see at short times a diffusive behavior, again with $\alpha=1$. At intermediate time scales we see the appearance of a plateau in the MSD ($\alpha\approx 0$). At a certain MSD, the energy associated with elastic deformation of the network becomes of the order of the thermal energy. As a result, the particles will be restricted to motion within this typical length scale, resulting in the plateau in the MSD. At longer time scales, due to the nonpermanent nature of the cross-links in these transient networks, we find a diffusive motion again. Similar experiments in covalently cross-linked polymer networks showed a plateau persisting up to the highest correlation times investigated (10^6 s) [30].

For sticking particles, as shown in Fig. 7(a), the same changes in the MSD at intermediate and long time scales are observed when the medium crosses the network formation threshold. However, we see an additional effect occurring at short correlation times (<0.1 ms). For these short times and for sticking particles we do not find diffusive motion, but a subdiffusive dynamics with $\langle \Delta r^2 \rangle \propto t^{1/2}$.

In the following sections we separately discuss the behavior in the three different regimes that can be distinguished in the dynamics of colloidal particles in transient networks: (i) the diffusive (nonsticking) and subdiffusive (sticking) motion at short time scales ($t<10^{-4}$ s), (ii) the caging plateau at intermediate time scales (10^{-4} s$<t<10^{-1}$ s), and (iii) the long-time diffusive behavior ($t>1$ s).

C. Short time scales

In Fig. 8 we have plotted the exponent α for the short-time ($t<10^{-4}$ s) dynamics of various combinations of particles and networks as a function of polymer concentration. We see that under sticking conditions (for plain silica particles) there is a transition from diffusive ($\alpha=1$) to subdiffusive motion with $\alpha=\frac{1}{2}$. This transition is found, for both the unmodified and associative polymer systems, at approximately twice the threshold concentration for network formation. For particles that are not bound to the surrounding network, this transition is absent. This is shown in Fig. 8 for the nonstick latex particles in entangled networks. For these particles the short-time motion remains diffusive over the entire concentration regime. These results strongly suggest that the typical exponent of $\frac{1}{2}$ is related to the binding of particles to the surrounding matrix and the presence of a network.

One special situation is also shown in Fig. 8 (squares) for particles with a preadsorbed layer of a high-molecular-weight PEO in associative networks. The associative polymer chains forming the network cannot adsorb onto these particles, so that we expect the particle not to show signs of

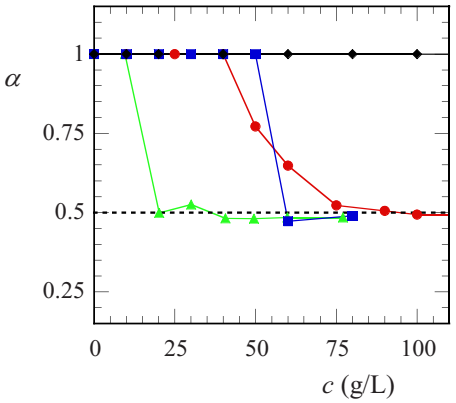

FIG. 8. (Color online) Effect of polymer concentration c on the exponent α [Eq. (1)] for short-time motion of particles in polymer networks. Four different combinations of probe particles and polymer are shown: silica particles (sticking) in solutions of unmodified PEO (●), silica particles (sticking) in solutions of hydrophobically modified, associative, polymer (▲), PEO-covered silica particles (special conditions, see text) in associative polymer solutions (■), and nonstick latex particles in regular PEO solutions (♦). The dotted line indicates α=0.5 for Rouse-like motion [20].

subdiffusive behavior. However, at higher concentrations entanglements also become important in the associative networks, in addition to the associative "cross-links" (i.e., micelles) between the chains. The adsorbed layer at the surface of the particle can probably take part in entanglements, and as a result, we see that the transition from diffusive to subdiffusive motion is delayed from twice the network threshold of the associative system (≈ 20 g/l) to a higher concentration where entanglements also become important (≈ 60 g/l). The transition for this special situation is found close to that of sticking particles in unmodified polymer solution. This indicates that entanglements become important at roughly the same concentration in the unmodified and in the modified systems.

A similar transition from diffusive to subdiffusive behavior upon changing the surface chemistry has been observed for particles in F-actin solutions by Chae and Furst [14]. These authors observed diffusive motion for nonsticky polystyrene probes preadsorbed with bovine serum albumin, while bare polystyrene beads displayed a MSD proportional to $t^{3/4}$. The exponent of 3/4 is related to the bending (or Rouse) modes of the semiflexible actin polymers. As we will show in the next section, the analogous Rouse modes for flexible chains lead to the $t^{1/2}$ scaling in the present work.

A physical interpretation of the short-time diffusive motion observed for nonsticking particles over the entire concentration range, even when there is a transient network surrounding the particles, is for example given in [6]. The nonsticking particles are surrounded by a depletion layer. At short times, when the particle displaces over small distances, the particles do not feel the surrounding network and exhibit a diffusive motion, with a corresponding diffusion coefficient that is of the same order of magnitude as the diffusion coefficient of these particles in the pure solvent. The short-time diffusion coefficient is slightly smaller than its pure solvent counterpart, though, because the flow field arising from the particle's Brownian motion is weakly perturbed by the surrounding network. A detailed analysis of such effects has been given by others [15,16,31,32].

In the following section we will develop a model that gives a physical interpretation of the subdiffusive short-time dynamics observed for sticking particles in transient networks.

D. Rouse model for colloids bound to polymer networks

As we discussed in a recent paper [20], the exponent $\alpha = \frac{1}{2}$ found for the short-time motion of sticking particles is indicative of Rouse-like behavior. We proposed a bead-spring model for the motion of a large particle anchored to a set of polymer chains to explain this scaling. Here, we provide a more detailed description of the model.

We consider a particle connected to f adsorbed polymer chains that are elastically active—i.e., connected to both the particle and a junction point in the polymer network (Fig. 9). The first segment in every chain m is connected to the particle, and the last segment N_m is fixed in a cross-link. For simplicity, we assume that $N_m = N$ is the same for all chains.

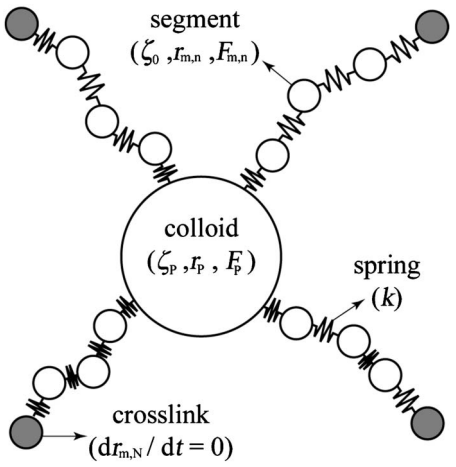

FIG. 9. Illustration of the proposed model of a colloidal particle (the large central bead) bound to several surrounding polymer chains (the bead-spring chains attached to the particle) that are part of a polymer network through the cross-links, here represented by the gray beads at the ends of the chains. In this illustration the number of adsorbed chains f is equal to 4 and the length of each chain part $N=4$ [20].

The equation of motion for a polymer segment in one of the adsorbed chains reads, neglecting inertia [33],

$$\zeta_0 \frac{dr_{m,n}}{dt} = -k(2r_{m,n} - r_{m,n-1} - r_{m,n+1}) + F_{m,n}, \tag{7}$$

where ζ_0 is the friction coefficient of a polymer segment, k is the spring constant of a bond between two monomers (related to the Kuhn length l_K by $k = 3k_BT/l_K^2$), $r_{m,n}$ denotes the position of segment n in chain m, and $F_{m,n}$ is the random force acting on that segment due to collisions with the solvent molecules. The colloidal particle is connected to f chains, so that its motion is described by

$$\zeta_P \frac{dr_P}{dt} = -k \sum_{m=1}^{f} (r_P - r_{m,1}) + F_p, \tag{8}$$

where $\zeta_P \gg \zeta_0$ is the friction coefficient of the particle and r_P its position. We assume that the chain ends can be considered fixed in space at the short time scales we are interested in here: $dr_{m,N}/dt = 0$. The random forces acting on the polymer segments and on the particle are assumed to be Gaussian and uncorrelated in time: $\langle F_{m,n}(t) \rangle = 0$ and $\langle F_{m,n}(t) F_{m',n'}(t') \rangle = 2k_BT\zeta_{m,n}\delta_{mm'}\delta_{nn'}\delta(t-t')$ according to the fluctuation dissipation theorem [33]. Equations (7) and (8) constitute a set of coupled differential equations that can be written in matrix form: $\dot{\mathbf{R}} = -\mathbf{A} \cdot \mathbf{R} + \mathbf{F}$. The solution is obtained by determining the eigenvalues and eigenvectors of the Rouse connectivity matrix $\mathbf{A}$ [34]. These can be obtained numerically, but for sufficiently long chains we can also obtain analytical expressions by taking a continuum limit. In the Appendix, we derive the MSD of the particle:

$$\langle \Delta r^2(t) \rangle = \frac{12 k_B T \chi^2 f}{k} \sum_{p=1}^{N} \frac{1 - \exp[-(\omega_p^2 k/\zeta_0)t]}{\omega_p^2 (N\omega_p^2 + N\chi^2 f^2 + \chi f)}, \quad (9)$$

where $\chi = \zeta_0/\zeta_P \ll 1$ is the size ratio between a polymer segment and the probe particle and where ω_p is determined by the characteristic equation $\omega_p \tan(\omega_p N) = \chi f$. For very weakly coupled particles, $N\chi f \ll 1$, the motion is dominated by the particle friction and the motion is diffusive until a plateau is reached. On the other hand, for $N\chi f > 1$, the connection with the polymer becomes important and the particle MSD shows three different regimes. At very short times ($t < \zeta_P^2/\zeta_0 k f^2$) the particle friction dominates and the MSD is diffusive: $\langle \Delta r^2(t) \rangle = 6 D_P t$, with $D_P = k_B T/\zeta_P$. Interestingly, at short time scales the particle motion is indeed Rouse-like, as observed in the experiments:

$$\langle \Delta r^2(t) \rangle = \frac{12 k_B T}{f(\zeta_0 k \pi)^{1/2}} t^{1/2}. \quad (10)$$

In this limit the prefactor does not depend on the friction coefficient of the particle. Hence, the bead just follows the motion of the polymer segments. Note that the MSD still depends on the particle radius R in this regime, as the number of adsorbed chains f is a function of R. At longer time scales $t \gg N\zeta_P/fk$, the MSD reaches a plateau, which depends on the number of adsorbed chains f and their length N:

$$\delta^2 = \lim_{t \to \infty} \langle \Delta r^2(t) \rangle = \frac{6 k_B T N}{fk}. \quad (11)$$

This expression for the mean-square plateau displacement δ^2 is a balance between the thermal energy $k_B T$ of the probe particle and the elastic energy in the surrounding network of polymer chains. Note that in our model the cross-links were assumed to be fixed, so that the long-time diffusive regime observed experimentally is not accounted for in this model.

The model above gives a microscopic explanation of both the short-time Rouse dynamics and the caging plateau at intermediate time scales. Relating these equations to measurable quantities is, however, somewhat troublesome due to the ingredients that were used, such as the number of elastically active adsorbed chains f and their length N. From Eqs. (10) and (11) we can see, however, that for a given system, the MSD for a given time t in the Rouse regime and for the mean-square plateau displacement should both scale with $1/f$.

In Fig. 10 we compare the MSD in the Rouse regime and at the caging plateau as a function of polymer concentration. We see that both quantities show approximately the same dependence on concentration. This implies that Eqs. (10) and (11) are consistent with our experimental data when we assume that all parameters in the model except f remain constant. The decrease in the MSD with polymer concentration then indicates that the number of adsorbed chains that are active in the network f increases with polymer concentration, which is expected. When the total number of chains in the system, as well as the number of junction points, increases, the number of chains that are connected to both a particle and a junction point in the network will also increase.

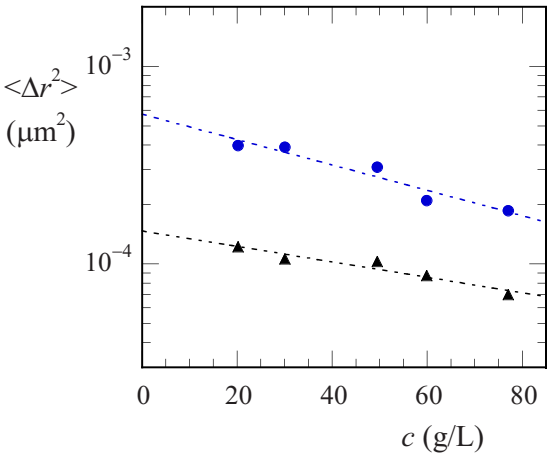

FIG. 10. (Color online) Comparison of the effect of polymer concentration on the MSD in the Rouse regime [at $t = 10^{-5}$ s (▲)] and at the caging plateau where $\alpha(t)$ [Eq. (1)] is minimal (●) for plain silica particles in associative networks. Dotted lines are drawn to guide the eye.

E. Intermediate time scales

The previous section gave a microscopic explanation of the short- and intermediate-time dynamics of colloidal particles in polymer networks. A more macroscopic consideration is derived by Mason and Weitz [1], who derived a generalized Stokes-Einstein equation that relates the MSD of a particle to the viscoelastic modulus $G^*(\omega)$ of the surrounding medium. In the plateau region, where $G^*(\omega) = G_0$, this gives, for the plateau MSD δ^2,

$$\delta^2 = \frac{k_B T}{6\pi R G_0}. \quad (12)$$

This expression is a macroscopic analog to Eq. (11).

The comparison between the true plateau displacement measured with DLS and the value predicted by Eq. (12), using the bulk plateau modulus as plotted in Fig. 5(b), is given in Fig. 11. We clearly see that the correspondence is very poor. The predicted value of δ^2 is a much stronger function of concentration ($\delta^2 \propto c^{-2.2}$) than the measured plateau displacement of the colloids ($\delta^2 \propto c^{-0.6}$). This was also observed previously for living polymer networks [6], where it was tentatively attributed to the existence of a depletion layer around the particle, which increases the actual cage size as experienced by the particles. Levine and Lubensky [32] developed a shell model that takes into account the presence of a depletion layer consisting of pure solvent, which was successfully applied to actin and DNA solutions [14–16]. In the present case, however, depletion effects cannot explain the deviations observed, as we find exactly the same plateau displacement for particles which stick to the network (and therefore should not have a depletion layer) and for particles that do not (which do have a depletion layer around them) (see Fig. 11).

Several other causes may be suggested to explain the strong deviations. First of all, as stated in the Introduction, it is the ratio of the dominant length scales, R/ξ, that is believed to determine whether the particle experiences a homo-

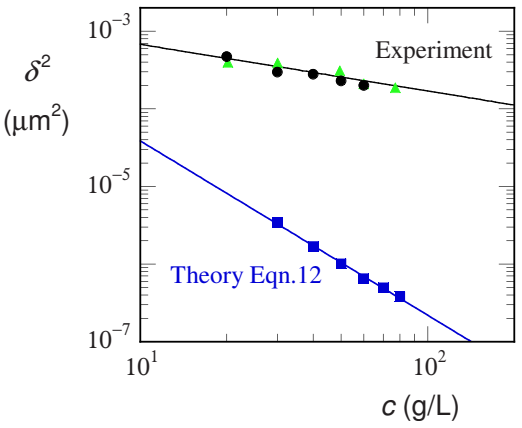

FIG. 11. (Color online) Effect of polymer concentration on the mean-square plateau displacement δ^2 from the DLS measurements, for plain silica particles (▲) and PEO-pretreated silica particles (●) in associative networks, and as obtained from Eq. (12) with the bulk plateau modulus shown in Fig. 5(b) (■). Drawn lines are power-law fits to the data.

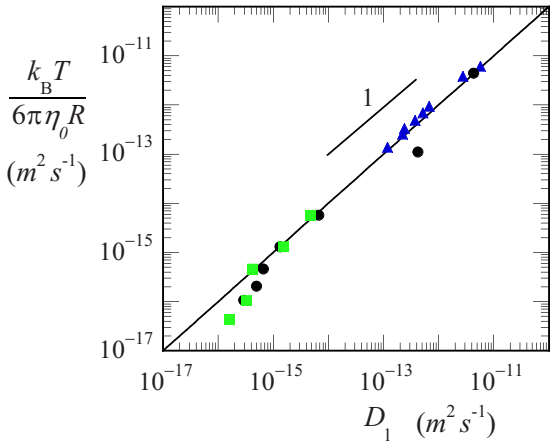

FIG. 12. (Color online) Stokes-Einstein diffusion coefficient, calculated with Eq. (14) and the bulk viscosity, versus the long-time diffusion coefficient obtained from the DLS experiments. For systems of (1) plain silica particles in entangled networks of unmodified PEO (▲), (2) plain silica particles in associative networks (■), and (3) silica particles, pretreated with a high-molecular-weight PEO, in associative networks (●). The drawn line represents $k_B T/6\pi\eta_0 R = D_l$.

geneous medium. For the systems studied here, R was either 70 or 110 nm. For polymer solutions above the overlap concentration (as used here), the correlation length must be smaller than the radius of gyration of the polymer coils, which is approximately 5 nm in this case. We therefore estimate $R/\xi \geq 10$. However, it is possible that the system shows structural and/or mechanical inhomogeneities on length scales larger than the particle size and/or particle displacement. If this is the case, the particles will preferentially probe the elastically weaker areas in the network, as there they are less restricted in their motion. The average elasticity that is experienced by the particles is then significantly smaller than the macroscopic elasticity, yielding a larger value of δ^2 than expected from Eq. (12). This is exactly what we observe in Fig. 11. Strangely, one would expect, when the bulk correlation length becomes smaller—i.e., with increasing polymer concentration—that the correspondence between the macroscopic prediction and the experimental results would also increase. However, we see that the deviation between the two grows with increasing concentration. This has also been observed by van der Gucht *et al.* [6].

Another explanation of the deviations might be in the assumption of a Maxwellian fluid. In Fig. 5(a), we can see that the Maxwell model does not accurately describe the viscoelastic response of the system at high frequencies. The frequency range that corresponds to the time scales of the caging plateau is not accessible at all with conventional bulk rheometry. As a result, we have to assume that the same parameters (G_0 and τ_0) that describe the experimentally accessible frequency range also describe the behavior at higher frequencies. It is conceivable that this assumption is not valid in this case and, as a result, could explain why Eq. (12) fails to describe our experimental data.

F. Long time scales

For the long-time diffusive motion, at time scales beyond the caging dynamics ($t > 1$ s), we define a diffusion coefficient D_l, given by [17]

$$D_l = \frac{d\langle \Delta r^2(t) \rangle}{6dt}. \tag{13}$$

The Stokes-Einstein equation predicts the diffusion coefficient of a spherical particles in a homogeneous liquid with viscosity η:

$$D = \frac{k_B T}{6\pi\eta R}. \tag{14}$$

In Fig. 12 we have plot, for various combinations of particles and networks, the diffusion coefficient calculated with Eq. (14), using the bulk viscosity (as shown in Fig. 4) versus the directly measured value of D_l [Eq. (13)]. Both approaches give, within the experimental uncertainty, the same value for the diffusion coefficient, as seen from the drawn line in Fig. 12, which represents $D_l = k_B T/6\pi\eta R$. The correspondence between the measured diffusion coefficient and the macroscopic prediction with the traditional Stokes-Einstein equation suggests that at these longer time scales the macroscopic properties of the networks dominate the particle dynamics.

IV. CONCLUSIONS

The thermal displacement of colloidal particles in transient polymer networks shows three distinct regimes: a slow diffusive motion at long time scales, an elastic caging plateau at intermediate time scales, and at short time scales either a fast diffusive motion for particles that do not stick to the surrounding network or Rouse-like dynamics for particles that are physically bound to the surrounding network. The behavior in these three regimes is addressed in this paper and the experimental findings are compared to microrheological models. We conclude that for short times, hence small displacements, the microscopic details of the medium and the

interactions between medium and particles are very important, whereas at very long time scales the motion seems governed by the bulk viscosity. For the short-time Rouse dynamics of particles bound to their surrounding polymer network, we have proposed an analytical model, which is found to be at least qualitatively consistent with the experimental results. The findings in this paper indicate that both of the central assumptions often made in microrheology—i.e., that particle-matrix interactions can be neglected and that the particles displace through a homogeneous medium—must be made with caution.

ACKNOWLEDGMENTS

The authors gratefully acknowledge Remco Fokkink and Hans de Rooij (Wageningen University) for constructing the homebuilt light-scattering setup, Dr. Søren Hvidt (Roskilde University) for performing the critical chromatography, and Anthonie Stuiver (Akzo Nobel Coatings Research, Sassenheim, the Netherlands) for providing the latex particles and assisting in preparing the associative polymers. The work of J.S. forms part of the research program of the Dutch Polymer Institute (DPI), Project No. 564.

APPENDIX

In this appendix we derive the MSD of a probe particle connected to a polymer network by solving Eqs. (7) and (8) in the continuum limit. The continuous analog of Eq. (7) is

$$\zeta_0 \frac{\partial r_m(n,t)}{\partial t} = k \frac{\partial^2 r_m(n,t)}{\partial n^2} + F_m(n,t), \tag{A1}$$

with boundary conditions at the fixed (cross-linked) end of the chain,

$$\frac{\partial r_m}{\partial t}(N,t) = 0, \tag{A2}$$

and at the bead,

$$\chi \sum_{m=1}^{f} \frac{\partial r_m}{\partial n}(0,t) = \frac{\partial^2 r_m}{\partial n^2}(0,t), \tag{A3}$$

where $\chi = \zeta_0/\zeta_P < 1$ is the size ratio between a polymer segment and the colloidal particle.

This partial differential equation can be solved by a transformation to normal coordinates,

$$r_m(n,t) = \sum_p R_{m,p}(n) X_p(t), \tag{A4}$$

where the eigenfunctions $R_{m,p}(n)$ are chosen such that

$$\frac{dX_p}{dt} = -\frac{1}{\tau_p} X_p + F_p, \tag{A5}$$

where τ_p is the relaxation time and F_p the effective random force for the modes. The general solution of Eq. (A5) is

$$X_p(t) = \int_{-\infty}^{t} \exp\left[-\frac{t-t'}{\tau_p}\right] F_p(t')dt'. \tag{A6}$$

From Eqs. (A1), (A4), and (A5), we find the following equations for the eigenfunctions:

$$\frac{d^2 R_{m,p}(n)}{dn^2} = -\omega_p^2 R_{m,p}(n), \tag{A7}$$

with

$$\omega_p^2 = \frac{\zeta_0}{k\tau_p}. \tag{A8}$$

Boundary condition (A3) becomes

$$\chi \sum_{m=1}^{f} \frac{dR_m}{dn}(0) = -\omega_p^2 R_m(0), \tag{A9}$$

and for the fixed chain end at $n=N$ we have $R_m(N)=0$. Equations (A7)–(A9) are the continuum version of the eigenvalue equations of the Rouse connectivity matrix **A**. There are two different types of solutions (normal modes). Antisymmetric modes $[R_p(n)=\sin(p\pi n/N)$ with $p=1,2,\ldots,N-1]$ have a node at $n=0$, so that the particle is stationary [34]. Hence, these modes do not contribute to the MSD of the particle. For the other modes we have

$$R_p(n) = \sin[\omega_p(n-N)], \tag{A10}$$

with ω_p given by the characteristic equation

$$\omega_p \tan(\omega_p N) = \chi f. \tag{A11}$$

Due to the slightly unusual boundary condition (A9), the eigenfunctions are not orthogonal. To proceed, we consider the elastic energy of the system [35]:

$$E[r] = \sum_{m=1}^{f} \frac{k}{2} \int_0^N \left(\frac{\partial r_m}{\partial n}\right)^2 dn = \sum_{p,q} X_p \alpha_{pq} X_q, \tag{A12}$$

where α_{pq} follows from Eqs. (A4) and (A10):

$$\alpha_{pq} = \frac{fk}{2} \int_0^N \frac{dR_p}{dn} \frac{dR_q}{dn} dn = \frac{fk\omega_p^2}{4} \left(N + \frac{\chi f}{(\chi f)^2 + \omega_p^2}\right) \delta_{pq}. \tag{A13}$$

Hence, even though the eigenfunctions $R_{m,p}$ are not orthogonal, the modes are statistically independent. Therefore, we can write the fluctuation dissipation theorem for the modes as

$$\langle F_p(t) f_q(t') \rangle = C_p \delta_{pq} \delta(t-t'), \tag{A14}$$

where C_p is a constant to be determined. From Eqs. (A6) and (A14), we find, for the mean-square amplitude of the modes,

$$\langle X_p^2(t) \rangle = \frac{C_p \zeta_0}{2k\omega_p^2}. \tag{A15}$$

In thermal equilibrium, the distribution of mode amplitudes must equal the Boltzmann distribution

$$P(X) \sim \exp[E[r]/k_BT] = \exp\left[\frac{1}{k_BT}\sum_p \alpha_{pp}X_p^2\right]. \quad \text{(A16)}$$

Hence, the modes are Gaussian distributed, with a mean-square amplitude $\langle X_p^2(t)\rangle = k_BT/2\alpha_{pp}$. Comparison to (A15) gives

$$C_p = \frac{k_BT\omega_p^2 k}{\zeta_0 \alpha_{pp}}. \quad \text{(A17)}$$

We can now derive the MSD of a segment:

$$\langle [r_{m,n}(t) - r_{m,n}(0)]^2\rangle = 3\sum_p R_{m,p}^2(n)\langle [X_p(t) - X_p(0)]^2\rangle$$
$$= \sum_p \frac{6}{\alpha_{pp}}(1 - e^{-k\omega_p^2 t/\zeta_0})\sin^2[\omega_p(n-N)], \quad \text{(A18)}$$

where the factor of 3 accounts for the three independent dimensions. For $n=0$ this reduces to the MSD of the probe particle, Eq. (9).

[1] T. G. Mason and D. A. Weitz, Phys. Rev. Lett. **74**, 1250 (1995).
[2] T. Gisler and D. A. Weitz, Curr. Opin. Colloid Interface Sci. **3**, 586 (1998).
[3] F. Gittes, B. Schnurr, P. D. Olmsted, F. C. MacKintosh, and C. F. Schmidt, Phys. Rev. Lett. **79**, 3286 (1997).
[4] F. C. Mackintosh and C. F. Schmidt, Curr. Opin. Colloid Interface Sci. **4**, 300 (1999).
[5] J. L. Harden and V. Viasnoff, Curr. Opin. Colloid Interface Sci. **6**, 438 (2001).
[6] J. van der Gucht, N. A. M. Besseling, W. Knoben, L. Bouteiller, and M. A. Cohen Stuart, Phys. Rev. E **67**, 051106 (2003).
[7] Y. Tseng, T. P. Kole, S. H. J. Lee, and D. Wirtz, Curr. Opin. Colloid Interface Sci. **7**, 210 (2002).
[8] E. M. Furst, Curr. Opin. Colloid Interface Sci. **10**, 79 (2005).
[9] J. H. van Zanten, S. Amin, and A. A. Abdala, Macromolecules **37**, 3874 (2004).
[10] Q. Lu and M. J. Solomon, Phys. Rev. E **66**, 061504 (2002).
[11] B. Schnurr, F. Gittes, P. Olmsted, F. C. Mackintosh, and C. F. Schmidt, Biophys. J. **72**, TU285 (1997).
[12] A. Caspi, M. Elbaum, R. Granek, A. Lachish, and D. Zbaida, Phys. Rev. Lett. **80**, 1106 (1998).
[13] A. J. Levine and F. C. MacKintosh, Phys. Rev. E **66**, 061606 (2002).
[14] B. S. Chae and E. M. Furst, Langmuir **21**, 3084 (2005).
[15] D. T. Chen, E. R. Weeks, J. C. Crocker, M. F. Islam, R. Verma, J. Gruber, A. J. Levine, T. C. Lubensky, and A. G. Yodh, Phys. Rev. Lett. **90**, 108301 (2003).
[16] J. Y. Huh and E. M. Furst, Phys. Rev. E **74**, 031802 (2006).
[17] A. Einstein, Ann. Phys. **17**, 549 (1905).
[18] J. H. van Zanten and K. P. Rufener, Phys. Rev. E **62**, 5389 (2000).
[19] I. Y. Wong, M. L. Gardel, D. R. Reichman, E. R. Weeks, M. T. Valentine, A. R. Bausch, and D. A. Weitz, Phys. Rev. Lett. **92**, 178101 (2004).
[20] J. Sprakel and J. van der Gucht, M. A. Cohen Stuart, and N. A. M. Besseling, Phys. Rev. Lett. **99**, 208301 (2007).
[21] Y. Serero, R. Aznar, G. Porte, J. F. Berret, D. Calvet, A. Collet, and M. Viguier, Phys. Rev. Lett. **81**, 5584 (1998).
[22] J. C. Dijt, M. A. C. Stuart, and G. J. Fleer, ACS Symp. Ser. **532**, 14 (1993).
[23] M. Santore and Z. Fu, Macromolecules **30**, 8516 (1997).
[24] R. Pecora, *Dynamic Light Scattering* (Plenum Press, New York, 1985).
[25] B. J. Berne and R. Pecora, *Dynamic Light Scattering* (Dover, Mineola, NY, 2000).
[26] T. Savin and P. S. Doyle, Biophys. J. **88**, 623 (2005).
[27] R. G. Larson, *The Structure and Rheology of Complex Fluids* (Oxford University Press, New York, 1998).
[28] T. Annable, R. Buscall, R. Ettelaie, and D. Whittlestone, J. Rheol. **37**, 695 (1993).
[29] F. Tanaka and S. F. Edwards, Macromolecules **25**, 1516 (1992).
[30] B. R. Dasgupta and D. A. Weitz, Phys. Rev. E **71**, 021504 (2005).
[31] T. H. Fan, J. K. G. Dhont, and R. Tuinier, Phys. Rev. E **75**, 011803 (2007).
[32] A. J. Levine and T. C. Lubensky, Phys. Rev. Lett. **85**, 1774 (2000).
[33] M. Doi and S. F. Edwards, *The Theory of Polymer Dynamics* (Clarendon Press, Oxford, 1986).
[34] B. H. Zimm and R. W. Kilb, J. Polym. Sci. **37**, 19 (1959).
[35] H. Qian, J. Math. Biol. **41**, 331 (2000).